A FUSION STRATEGY TO MAP CORN CROP RESIDUES

Fathololoumi S[1], Firozjaei K.M[2], Daggupati P[3], and Biswas A[1]*

[1] School of Environmental Sciences, University of Guelph, Canada

[2] Department of Remote Sensing and GIS, Faculty of Geography, University of Tehran, Tehran, Iran

[3] School of Engineering, University of Guelph, Canada

Emails: sfatholo@uoguelph.ca; mohammad.karimi.f@ut.ac.ir; pdaggupa@uoguelph.ca; biswas@uoguelph.ca

*Correspondence: Asim Biswas

Abstract

Access to post-harvest residue coverage information is crucial for agricultural management and soil conservation. The purpose of this study was to present a new approach based on an ensemble at the decision level for mapping the corn residue. To this end, a set of Landsat 8 and Sentinel-1 imagery, and field data including the Residue Cover Fraction (RCF) of corn (149 samples), were used. Firstly, a map of common spectral indices for RCF modeling was prepared based on the spectral bands. Then, the efficiency of each index in RCF mapping was evaluated. Secondly, the efficiency of three machine learning algorithms including Artificial Neural Networks (ANN), Random Forest (RF), and Support Vector Regression (SVR) was evaluated and compared with each other. Furthermore, to increase the accuracy of RCF mapping, different algorithm results were combined based on their modeling error, which is called the ensemble approach. The results showed that the coefficient of determination (R) between the Broadband spectral Angle Index (BAI) and RCF was 0.63, which was higher than other spectral indices. The R(RMSE) between the actual and modeled RCF based on ANN, RF, and SVR algorithms using spectral indices were 0.83 (3.89), 0.86(3.25), and 0.76 (4.56), respectively. By applying the ensemble approach, the error of RCF mapping was reduced by 0.85% compared to the results of the best machine learning algorithm. The results showed that the ensemble approach improved the accuracy of the RCF mapping significantly.

Keywords.

Reflective and radar bands, Corn residue; ensemble, Machine learning algorithm.

Introduction

The health of the soil can be harmed by agricultural practices like plowing and tillage, which involves heavy machinery. This damage increases the soil's susceptibility to rain-induced soil erosion, which results in the loss of the topsoil layer that is vital to crop growth (Liao et al. 2022).

The eroding soil frequently finds its way into rivers, where it contaminates the water with substances like phosphorous (Maruffi et al. 2022). Deteriorating soil quality also causes the release of precipitated carbon, which raises atmospheric carbon dioxide concentrations and fuels climate change. Keeping post-harvest vegetation on the soil surface is a practical and efficient way to reduce soil erosion and increase soil productivity (Han et al. 2023).

Crop residues are crucial in maintaining soil health as they remain on the field following harvest. Crop residue influence the chemical, physical, and biological characteristics of the soil, lowering evaporation, improving water permeability, and raising crop production (Turmel et al. 2015). Furthermore, by limiting the release of gases like NH_3, CO, and SO_2 that arise from burning plant wastes, their preservation can help lower air pollution (Singh et al. 2020).

Mapping crop residue is essential for sustainable agricultural goals, including environmental health. Broad-scale field trips and sampling are impracticable for traditional approaches; remote sensing (RS) techniques, on the other hand, are highly accurate for assessing agricultural residues across broad areas (Zheng et al. 2014). Previous research has modelled residue cover fraction (RCF) using a variety of satellite images, including Landsat (Hively et al. 2019), Sentinel-2 (Gao et al. 2022), and RADARSAT (Cai et al. 2019), in addition to a number of RS indices. Although these indices have benefits and drawbacks, their efficacy varies according to the surrounding circumstances.

Complex agricultural landscapes frequently challenge single indices, which is why multivariate regression techniques like Random Forest Regression (RFR), Support Vector Regression (SVR), and Artificial Neural Networks (ANN) are used to improve RCF modeling (Ding et al. 2020). However, RCF modeling accuracy can be greatly increased by combining the capabilities of several models and indices. This paper offers a new method for mapping corn residue that is based on an ensemble at the decision level.

2. Study area

Ontario is a key agricultural area in Canada, known for its wide variety of crops and orchards. For this research, an area in southern Ontario was chosen, located at 82.5° west and 42.5° north. This area predominantly grows corn, wheat, and soybeans (Figure 1). Covering roughly 4324 km², the region has 1218 km² allocated to corn farming. Given the climate and long winters, most crops here are harvested by September.

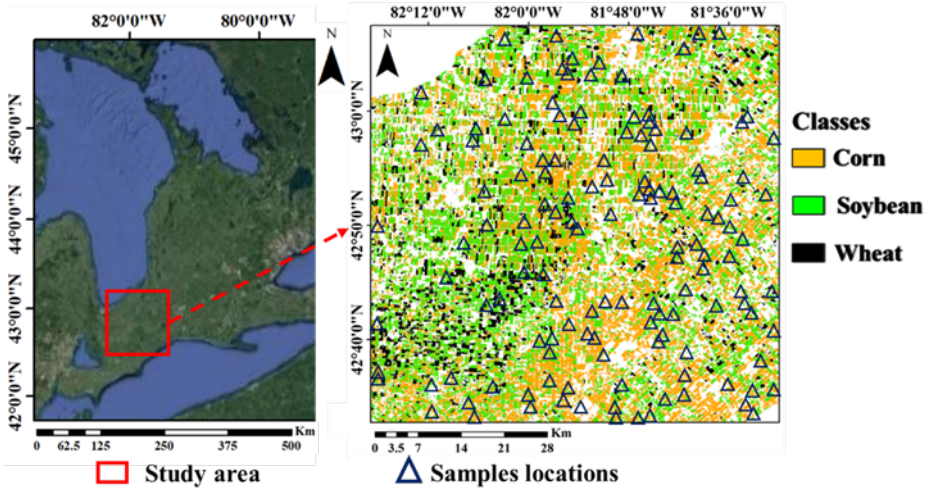

Figure 1. Geographical location (left) and the land crop classes of the study area (right).

3. Data and methods

3.1. Data

To evaluate multiple models and datasets in RCF modeling, a set of Landsat 8 and Sentinel-1 imagery bands and indices, and field data including corn Residue Cover Fraction (RCF) (149 samples), were used. Additionally, a land cover map created by Agriculture and Agri-Food Canada (AAFC) in 2020 (30 m), was used to mask corn from various agricultural products.

Ground data collection was carried out post-harvest and involved calculating the RCF in the fall from multiple corn fields. Corn RCF values were measured at 149 locations for this purpose. A Phantom 3 SE drone was utilized to take pictures from each chosen sample site, and camera photographs were used in sampling process. At each sampling site, a digital orthophoto produced with a spatial resolution of 20 cm while the drone was in the air at a height of 20 m. After that, each image's crop residue location was manually digitalized. The RCF was computed for an area of 900 m² surrounding each sampling point after the camera images were processed.

3.2. Methods

First, based on the satellite bands, a map of spectral indices was created. Then, the AAFC map was used to mask these maps to Corn crop fields. Next, the effectiveness of several algorithms such as SVM, RFR, and ANN was assessed and contrasted with one another. To further improve the accuracy of modeling, the output of various algorithms was integrated based on the modeling error.

3.2.1. Effective Variables

For RCF modeling, a number of spectral indices have been created in earlier works, including STI, DFI, NDVI, NDSVI, NDTI, NDI5, NDI7, 3BI3, and BAI. Backscatter data from the VV and VH bands of Sentinel-1 were also utilized (Table 1).

Table 1. Utilized bands and indices.

Type	Spectral Indices	Equation	Reference
Spectral indices	DFI	100×(1 − OLI7/OLI6)×(OLI4/OLI5)	(Bocco et al. 2014)
	STI	OLI6/OLI7	(Van Deventer et al. 1997)
	NDSVI	(OLI6 − OLI4)/(OLI6 + OLI4)	(Qi et al. 2002)
	NDTI	(OLI6 − OLI7)/(OLI6 + OLI7)	(Van Deventer et al. 1997)
	NDI5	(OLI5 − OLI6)/(OLI5 + OLI6)	(McNairn and Protz 1993)
	NDI7	(OLI5 − OLI7)/(OLI5 + OLI7)	(McNairn and Protz 1993)
	NDVI	(OLI5 − OLI4)/(OLI5 + OLI4)	(Ding et al. 2020)
	3BI3	(OLI7 − OLI4)/(OLI7 + OLI6)	(Ding et al. 2020)
	BAI	-	(Yue et al. 2020)
Backscatter bands	VV	-	-
	VH	-	-

3.2.2. Machine Learning Methods

The RCF was modeled using multivariate modeling algorithms, namely RFR, SVM, and ANN. All reflective band-based spectral indices were employed as independent variables in the first strategy. In the second strategy, the modeling process incorporated VV and VH band information along with spectral indices derived from reflective bands. The 96 samples of training data were used to calibrate each RFR, SVM, and ANN algorithm. Next, utilizing test data (53 samples), the effectiveness of each of these algorithms was assessed.

3.2.3. Decision-based ensemble approach

Equation (1) used in the proposed strategy to integrate the output of RFR, SVM, and ANN

algorithms in order to reduce the error of the modeled RCF based on RS data.

$$RCF_f = \sum_{i=1}^{n} W_i RCF_{model(i)} \quad (1)$$

Wi denotes the algorithm's degree of importance, n is the number of used algorithms, $RCF_{model(i)}$ is the fraction of the modeled RCF based on the RS data obtained from the i_{th} algorithm, and RCF_f is the modeled RCF based on the data obtained by combining the results of different algorithms. The i_{th} algorithm's significance is computed using equation (2).

$$W_i = \frac{RMSE_{model(i)}}{\sum_{i=1}^{n} RMSE_{model(i)}} \quad (2)$$

Equation (2) uses the i_{th} technique to calculate $RMSE_{model(i)}$, which is the root mean square error of the estimated fraction. An algorithm's impact and significance on the RCF estimate result increase with decreasing RMSE.

4. Results

According to Table 2, the effectiveness of spectral indices based on reflective bands varied. Compared to other spectral indices, the R^2 between BAI and the residues was higher at 0.63. The R^2 value between the VV band and the residues was 0.25, and for the VH band, it was 0.29. The radar bands were less efficient compared to the spectral indices.

Table 2. The R^2 between the effective variables and residue.

Effective variables	R^2
3BI3	0.46
NDI5	0.54
NDI7	0.60
NDSVI	0.07
NDTI	0.42
NDVI	0.43
STI	0.43
DFI	0.55
BAI	0.63
VV	0.25
VH	0.29

The validation data showed that the R^2 (RMSE) was 0.83 (3.89), 0.86 (3.25), and 0.76 (4.56), between the actual and modeled RCF based on ANN, RFR, and SVR algorithms, respectively (Figure 2). According to the findings, the RFR algorithm exhibited the highest level of accuracy.

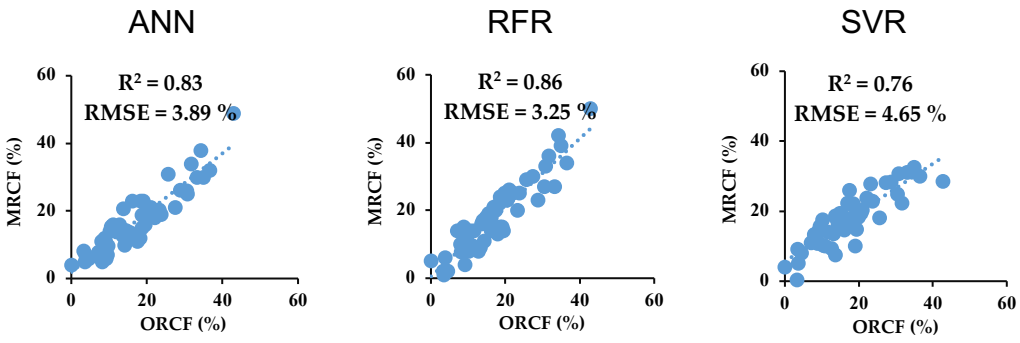

Figure 2. R^2 and RMSE between actual and model RCF based on validation data.

When spectral indices and radar bands considered together as dependent variables, the R^2 (RMSE) between the real and modeled values of the corn RCF based on ANN, RFR, and SVR algorithms was 0.85 (3.45), 0.89 (2.68), and 0.80 (4.02%).

According to the ensemble strategy, the R^2 (RMSE) between the modeled and actual RCF was 0.92 (1.78) % (Figure 3). In comparison to the outcomes of the best ML algorithm, the model error based on the suggested technique was decreased by 0.90 %.

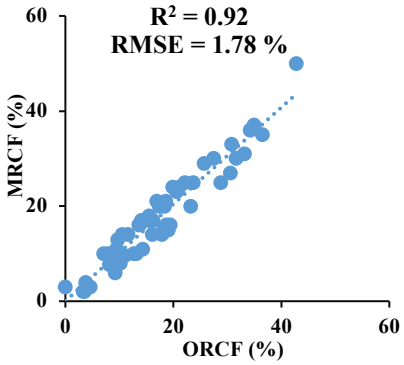

Figure 3. R^2 and RMSE between the actual and modeled RCF based on the proposed strategy. ORCF is the observed RCF and MRCF is the modeled RCF.

The RCF map created using the suggested approach revealed that the residue's spatial distribution differed throughout the research region (Figure 4). The RCF ranged from 0% to 62%. The study area's eastern farms had a lower RCF than its western farms. The highest residue values were found in the research area's northwest corn fields. The research area's average RCF was 18.2%. In the study area, the RCF's standard deviation (Sd) was 8.3%.

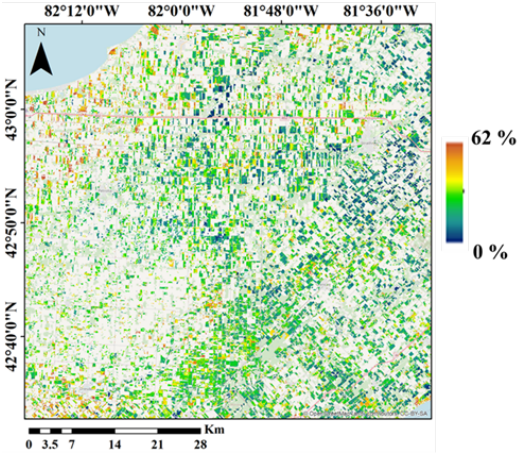

Figure 4. Corn RCF map for the study area.

5. Conclusion

Crop residue mapping is essential for sustainable agriculture as it aids in managing soil health, reducing erosion, and enhancing nutrient cycling. RS data is particularly valuable for this purpose due to its ability to provide extensive, timely, and accurate coverage of large agricultural areas. Nevertheless, a number of variables, such as (1) the dependent variables used in the modeling process, (2) the calibration and validation data quality, and (3) the algorithms used to build the appropriate model between the effective variables and the RCF, affect how accurately different crops are mapped to the RCF using satellite data (Ding et al. 2020; Yue et al. 2020). The impact of dependent variables and the algorithms utilized in the RCF modeling procedure examined in this study. A new approach based on the ensemble of several ML algorithms' results at the decision level was created to increase the accuracy of RCF modeling and mapping. Out of all the ML methods, RFR accuracy outperformed the others. The accuracy of RCF modeling improved with the ensemble of outcomes from several ML algorithms at the decision level. It is recommended that the effectiveness of deep learning algorithms in RCF modeling be assessed in subsequent research.

References

Baghdadi, N., El Hajj, M., & Zribi, M. (2019). An operational high resolution soil moisture retrieval algorithm using

sentinel-1 images. In, *2019 PhotonIcs & Electromagnetics Research Symposium-Spring (PIERS-Spring)* (pp. 4086-4092): IEEE

Bryant, R., Moran, M.S., Thoma, D., Collins, C.H., Skirvin, S., Rahman, M., Slocum, K., Starks, P., Bosch, D., & Dugo, M.G. (2007). Measuring surface roughness height to parameterize radar backscatter models for retrieval of surface soil moisture. *Ieee Geoscience and Remote Sensing Letters, 4*, 137-141

de Queiroz, M.G., da Silva, T.G.F., Zolnier, S., Jardim, A.M.d.R.F., de Souza, C.A.A., Júnior, G.d.N.A., de Morais, J.E.F., & de Souza, L.S.B. (2020). Spatial and temporal dynamics of soil moisture for surfaces with a change in land use in the semi-arid region of Brazil. *Catena, 188*, 104457

El Hajj, M., Baghdadi, N., & Zribi, M. (2019). Comparative analysis of the accuracy of surface soil moisture estimation from the C-and L-bands. *International Journal of Applied Earth Observation and Geoinformation, 82*, 101888

Fathololoumi, S., Firozjaei, M.K., & Biswas, A. (2022). Improving spatial resolution of satellite soil water index (SWI) maps under clear-sky conditions using a machine learning approach. *Journal of hydrology, 615*, 128709

Fathololoumi, S., Vaezi, A.R., Alavipanah, S.K., Ghorbani, A., & Biswas, A. (2020). Comparison of spectral and spatial-based approaches for mapping the local variation of soil moisture in a semi-arid mountainous area. *Science of the Total Environment, 724*, 138319

Fathololoumi, S., Vaezi, A.R., Firozjaei, M.K., & Biswas, A. (2021). Quantifying the effect of surface heterogeneity on soil moisture across regions and surface characteristic. *Journal of hydrology, 596*, 126132

Greifeneder, F., Notarnicola, C., Hahn, S., Vreugdenhil, M., Reimer, C., Santi, E., Paloscia, S., & Wagner, W. (2018). The added value of the VH/VV polarization-ratio for global soil moisture estimations from scatterometer data. *IEEE Journal of Selected Topics in Applied Earth Observations and Remote Sensing, 11*, 3668-3679

Guan, X., Huang, J., Guo, N., Bi, J., & Wang, G. (2009). Variability of soil moisture and its relationship with surface albedo and soil thermal parameters over the Loess Plateau. *Advances in Atmospheric Sciences, 26*, 692-700

Jiang, K., Pan, Z., Pan, F., Wang, J., Han, G., Song, Y., Zhang, Z., Huang, N., Ma, S., & Chen, X. (2022). Influence patterns of soil moisture change on surface-air temperature difference under different climatic background. *Science of the Total Environment, 822*, 153607

Kornelsen, K.C., & Coulibaly, P. (2013). Advances in soil moisture retrieval from synthetic aperture radar and hydrological applications. *Journal of hydrology, 476*, 460-489

Li, H., Van den Bulcke, J., Mendoza, O., Deroo, H., Haesaert, G., Dewitte, K., De Neve, S., & Sleutel, S. (2022). Soil texture controls added organic matter mineralization by regulating soil moisture—evidence from a field experiment in a maritime climate. *Geoderma, 410*, 115690

Liu, M., Adam, J.C., Richey, A.S., Zhu, Z., & Myneni, R.B. (2018). Factors controlling changes in evapotranspiration, runoff, and soil moisture over the conterminous US: Accounting for vegetation dynamics. *Journal of hydrology, 565*, 123-137

Merlin, O., Olivera-Guerra, L., Hssaine, B.A., Amazirh, A., Rafi, Z., Ezzahar, J., Gentine, P., Khabba, S., Gascoin, S., & Er-Raki, S. (2018). A phenomenological model of soil evaporative efficiency using surface soil moisture and temperature data. *Agricultural and forest meteorology, 256*, 501-515

Orth, R. (2021). Global soil moisture data derived through machine learning trained with in-situ measurements. *Scientific data, 8*, 1-14

Paloscia, S., Pettinato, S., Santi, E., Notarnicola, C., Pasolli, L., & Reppucci, A. (2013). Soil moisture mapping using Sentinel-1 images: Algorithm and preliminary validation. *Remote Sensing of Environment, 134*, 234-248

Romano, N. (2014). Soil moisture at local scale: Measurements and simulations. *Journal of hydrology, 516*, 6-20

Sun, H., Zhou, B., & Liu, H. (2019). Spatial evaluation of soil moisture (SM), land surface temperature (LST), and LST-derived SM indexes dynamics during SMAPVEX12. *Sensors, 19*, 1247

Xia, L., Song, X., Leng, P., Wang, Y., Hao, Y., & Wang, Y. (2019). A comparison of two methods for estimating surface soil moisture based on the triangle model using optical/thermal infrared remote sensing over the source area of the Yellow River. *International Journal of Remote Sensing, 40*, 2120-2137

Zhao, W., Sanchez, N., & Li, A. (2018). Triangle Space-Based Surface Soil Moisture Estimation by the Synergistic Use of $ In\Situ $ Measurements and Optical/Thermal Infrared Remote Sensing: An Alternative to Conventional Validations. *Ieee Transactions on Geoscience and Remote Sensing, 56*, 4546-4558

Zribi, M., Le Hégarat-Mascle, S., Ottlé, C., Kammoun, B., & Guerin, C. (2003). Surface soil moisture estimation from the synergistic use of the (multi-incidence and multi-resolution) active microwave ERS Wind Scatterometer and SAR data. *Remote Sensing of Environment, 86*, 30-41

Akıncı, H., Özalp, A.Y., & Turgut, B. (2013). Agricultural land use suitability analysis using GIS and AHP technique. *Computers and electronics in agriculture, 97*, 71-82

Bodner, G., Scholl, P., Loiskandl, W., & Kaul, H.-P. (2013). Environmental and management influences on temporal variability of near saturated soil hydraulic properties. *Geoderma, 204*, 120-129

Crow, W.T., Berg, A.A., Cosh, M.H., Loew, A., Mohanty, B.P., Panciera, R., de Rosnay, P., Ryu, D., & Walker, J.P. (2012). Upscaling sparse ground-based soil moisture observations for the validation of coarse-resolution satellite soil moisture products. *Reviews of Geophysics, 50*

Delelegn, Y.T., Purahong, W., Blazevic, A., Yitaferu, B., Wubet, T., Göransson, H., & Godbold, D.L. (2017). Changes in

land use alter soil quality and aggregate stability in the highlands of northern Ethiopia. *Scientific Reports, 7*, 13602

Fathololoumi, S., Vaezi, A.R., Alavipanah, S.K., Ghorbani, A., Saurette, D., & Biswas, A. (2021). Effect of multi-temporal satellite images on soil moisture prediction using a digital soil mapping approach. *Geoderma, 385*, 114901

Jalali, M. (2007). Phosphorus status and sorption characteristics of some calcareous soils of Hamadan, western Iran. *Environmental Geology, 53*, 365-374

Jiang, Y., & Weng, Q. (2017). Estimation of hourly and daily evapotranspiration and soil moisture using downscaled LST over various urban surfaces. *GIScience & remote sensing, 54*, 95-117

Lenka, N., Choudhury, P., Sudhishri, S., Dass, A., & Patnaik, U. (2012). Soil aggregation, carbon build up and root zone soil moisture in degraded sloping lands under selected agroforestry based rehabilitation systems in eastern India. *Agriculture, ecosystems & environment, 150*, 54-62

Paul, B.K., Vanlauwe, B., Ayuke, F., Gassner, A., Hoogmoed, M., Hurisso, T., Koala, S., Lelei, D., Ndabamenye, T., & Six, J. (2013). Medium-term impact of tillage and residue management on soil aggregate stability, soil carbon and crop productivity. *Agriculture, ecosystems & environment, 164*, 14-22

Riihimäki, H., Kemppinen, J., Kopecký, M., & Luoto, M. (2021). Topographic wetness index as a proxy for soil moisture: The importance of flow-routing algorithm and grid resolution. *Water Resources Research, 57*, e2021WR029871

Xiang, X., Wu, X., Chen, X., Song, Q., & Xue, X. (2017). Integrating topography and soil properties for spatial soil moisture storage modeling. *Water, 9*, 647

Fathololoumi, S., Vaezi, A.R., Alavipanah, S.K., Ghorbani, A., Saurette, D., & Biswas, A. (2021). Effect of multi-temporal satellite images on soil moisture prediction using a digital soil mapping approach. *Geoderma, 385*, 114901

Malone, B.P., Minasny, B., McBratney, A.B., Malone, B.P., Minasny, B., & McBratney, A.B. (2017). Some methods for the quantification of prediction uncertainties for digital soil mapping. *Using R for digital soil mapping*, 169-219

Bocco, M., Sayago, S., & Willington, E. (2014). Neural network and crop residue index multiband models for estimating crop residue cover from Landsat TM and ETM+ images. *International Journal of Remote Sensing, 35*, 3651-3663

Cai, W., Zhao, S., Wang, Y., Peng, F., Heo, J., & Duan, Z. (2019). Estimation of winter wheat residue coverage using optical and SAR remote sensing images. *Remote Sensing, 11*, 1163

Ding, Y., Zhang, H., Wang, Z., Xie, Q., Wang, Y., Liu, L., & Hall, C.C. (2020). A comparison of estimating crop residue cover from sentinel-2 data using empirical regressions and machine learning methods. *Remote Sensing, 12*, 1470

Gao, L., Zhang, C., Yun, W., Ji, W., Ma, J., Wang, H., Li, C., & Zhu, D. (2022). Mapping crop residue cover using Adjust Normalized Difference Residue Index based on Sentinel-2 MSI data. *Soil and Tillage Research, 220*, 105374

Han, J., Pan, Y., Xiao, P., Ge, W., & Sun, P. (2023). Quantifying the effects of climate change and revegetation on erosion-induced lateral soil organic carbon loss on the Chinese Loess Plateau. *Remote Sensing, 15*, 1775

Hively, W.D., Shermeyer, J., Lamb, B.T., Daughtry, C.T., Quemada, M., & Keppler, J. (2019). Mapping crop residue by combining Landsat and WorldView-3 satellite imagery. *Remote Sensing, 11*, 1857

Liao, Y., Zhang, B., Kong, X., Wen, L., Yao, D., Dang, Y., & Chen, W. (2022). A cooperative-dominated model of conservation tillage to mitigate soil degradation on cultivated land and its effectiveness evaluation. *Land, 11*, 1223

Maruffi, L., Stucchi, L., Casale, F., & Bocchiola, D. (2022). Soil erosion and sediment transport under climate change for Mera River, in Italian Alps of Valchiavenna. *Science of the Total Environment, 806*, 150651

McNairn, H., & Protz, R. (1993). Mapping corn residue cover on agricultural fields in Oxford County, Ontario, using Thematic Mapper. *Canadian Journal of Remote Sensing, 19*, 152-159

Qi, J., Marsett, R., Heilman, P., Bieden-bender, S., Moran, S., Goodrich, D., & Weltz, M. (2002). RANGES improves satellite-based information and land cover assessments in southwest United States. *Eos, Transactions American Geophysical Union, 83*, 601-606

Singh, R., Yadav, D.B., Ravisankar, N., Yadav, A., & Singh, H. (2020). Crop residue management in rice–wheat cropping system for resource conservation and environmental protection in north-western India. *Environment, Development and Sustainability, 22*, 3871-3896

Turmel, M.-S., Speratti, A., Baudron, F., Verhulst, N., & Govaerts, B. (2015). Crop residue management and soil health: A systems analysis. *Agricultural Systems, 134*, 6-16

Van Deventer, A., Ward, A., Gowda, P., & Lyon, J. (1997). Using thematic mapper data to identify contrasting soil plains and tillage practices. *Photogrammetric Engineering and Remote Sensing, 63*, 87-93

Yue, J., Tian, Q., Dong, X., & Xu, N. (2020). Using broadband crop residue angle index to estimate the fractional cover of vegetation, crop residue, and bare soil in cropland systems. *Remote Sensing of Environment, 237*, 111538

Zheng, B., Campbell, J.B., Serbin, G., & Galbraith, J.M. (2014). Remote sensing of crop residue and tillage practices: Present capabilities and future prospects. *Soil and Tillage Research, 138*, 26-34